



Article

# Application of Box–Behnken Design to Optimize Phosphate Adsorption Conditions from Water onto Novel Adsorbent CS-ZL/ZrO/Fe<sub>3</sub>O<sub>4</sub>: Characterization, Equilibrium, Isotherm, Kinetic, and Desorption Studies

Endar Hidayat <sup>1,2</sup> , Nur Maisarah Binti Mohamad Sarbani <sup>1,2</sup>, Seiichiro Yonemura <sup>1,2</sup>, Yoshiharu Mitoma <sup>1,2</sup> and Hiroyuki Harada <sup>1,2,\*</sup>

- <sup>1</sup> Graduate School of Comprehensive and Scientific Research, Prefectural University of Hiroshima, Shobara 727-0023, Japan; hidayatendar1@gmail.com (E.H.)  
<sup>2</sup> Department of Life and Environmental Science, Faculty of Bioresources Science, Prefectural University of Hiroshima, Shobara 727-0023, Japan  
\* Correspondence: ho-harada@pu-hiroshima.ac.jp

**Abstract:** Phosphate (PO<sub>4</sub><sup>3-</sup>) is an essential nutrient in agriculture; however, it is hazardous to the environment if discharged in excess as in wastewater discharge and runoff from agriculture. Moreover, the stability of chitosan under acidic conditions remains a concern. To address these problems, CS-ZL/ZrO/Fe<sub>3</sub>O<sub>4</sub> was synthesized using a crosslinking method as a novel adsorbent for the removal of phosphate (PO<sub>4</sub><sup>3-</sup>) from water and to increase the stability of chitosan. The response surface methodology (RSM) with a Box–Behnken design (BBD)-based analysis of variance (ANOVA) was implemented. The ANOVA results clearly showed that the adsorption of PO<sub>4</sub><sup>3-</sup> onto CS-ZL/ZrO/Fe<sub>3</sub>O<sub>4</sub> was significant ( $p \leq 0.05$ ), with good mechanical stability. pH, dosage, and time were the three most important factors for the removal of PO<sub>4</sub><sup>3-</sup>. Freundlich isotherm and pseudo-second-order kinetic models generated the best equivalents for PO<sub>4</sub><sup>3-</sup> adsorption. The presence of coexisting ions for PO<sub>4</sub><sup>3-</sup> removal was also studied. The results indicated no significant effect on PO<sub>4</sub><sup>3-</sup> removal ( $p \leq 0.05$ ). After adsorption, PO<sub>4</sub><sup>3-</sup> was easily released by 1 M NaOH, reaching 95.77% and exhibiting a good capability over three cycles. Thus, this concept is effective for increasing the stability of chitosan and is an alternative adsorbent for the removal of PO<sub>4</sub><sup>3-</sup> from water.

**Keywords:** phosphate adsorption; zeolite; chitosan; ZrO; Fe<sub>3</sub>O<sub>4</sub>; Box–Behnken design; mechanical stability



**Citation:** Hidayat, E.; Mohamad Sarbani, N.M.B.; Yonemura, S.; Mitoma, Y.; Harada, H. Application of Box–Behnken Design to Optimize Phosphate Adsorption Conditions from Water onto Novel Adsorbent CS-ZL/ZrO/Fe<sub>3</sub>O<sub>4</sub>: Characterization, Equilibrium, Isotherm, Kinetic, and Desorption Studies. *Int. J. Mol. Sci.* **2023**, *24*, 9754. <https://doi.org/10.3390/ijms24119754>

Academic Editors: Swarup Roy and Valentina Siracusa

Received: 11 May 2023

Revised: 31 May 2023

Accepted: 1 June 2023

Published: 5 June 2023



**Copyright:** © 2023 by the authors. Licensee MDPI, Basel, Switzerland. This article is an open access article distributed under the terms and conditions of the Creative Commons Attribution (CC BY) license (<https://creativecommons.org/licenses/by/4.0/>).

## 1. Introduction

Phosphate (PO<sub>4</sub><sup>3-</sup>) is a macronutrient needed for plant growth and is frequently applied as a fertilizer on agricultural lands. The increasing demands of food supply nowadays have led to the excessive application of fertilizer. However, excessive fertilizer use can cause PO<sub>4</sub><sup>3-</sup> to leach into waterways, leading to eutrophication and harmful algal bloom. These blooms diminish oxygen levels [1–3], interfere with aquatic life, and adversely affect the quality of drinking water (taste and odor) [4]. According to [5], PO<sub>4</sub><sup>3-</sup> decontamination must be performed efficiently while having a minimal impact on the surrounding ecosystem. Many methods have been reported to be effective in removing PO<sub>4</sub><sup>3-</sup> from water, including biological [6] methods, electrochemical [7,8] methods, precipitation [9], ion exchange [10], and adsorption [11,12]. Each strategy has advantages and disadvantages. Biological techniques are more economical; however, the residue of dead bacteria left behind after the process is inconvenient [13]. Electrochemical techniques are expensive but have a lower effectivity toward PO<sub>4</sub><sup>3-</sup> removal [14]. The precipitation process is simple

and effective for chemical treatment but is inefficient for sewage sludge and waste disposal [15]. Ion exchange may also be used to remove anions by exchanging sulfates ( $\text{SO}_4^{2-}$ ) for  $\text{PO}_4^{3-}$  ions; however, this would make the solution more corrosive, and it requires a costly clean-up (Blaney et al. [16]). Adsorption is the best option and is the most widely used method for water contaminants including  $\text{PO}_4^{3-}$  ions [17,18]. This is because the technique is environmentally safe, the operation is easy and fast, and the technology is highly efficient.

Chitosan is currently gaining popularity as a potential adsorbent for water contaminants because it contains hydroxyl ( $-\text{OH}$ ) and amino ( $-\text{NH}_2$ ) functional groups, which can easily react with other materials and are environmentally friendly [19]. This material, which cannot be accessed readily from nature, is synthesized through the chemical deacetylation of chitin. However, because of its low tensile strength and dissolution under acidic conditions, the use of chitosan directly in wastewater treatment technologies is not recommended. Therefore, chitosan must be modified to increase its chemical stability and adsorption capability [20]. The selection of an appropriate modification method and modifying agent is crucial for assessing the quality and functionality of the product created during the modification process. Crosslinking is one of the most frequently used procedures to enhance the physicochemical characteristics of chitosan [21,22]. Crosslinking is the process of combining two or more molecules via covalent bonds.

Zeolites are crystalline aluminum silicate ( $\text{Al}_2\text{O}_3 \cdot 2\text{SiO}_2$ ) minerals with a porous and highly stable structure, and they could enhance the adsorption of chitosan onto their surface, leading to the improved stability of chitosan. These materials can be obtained from natural sources, such as shrimp, or can be synthesized using various methods [23]. Several reports have proven the use of chitosan and zeolite to remove dyes [24,25], pharmaceuticals [26], nitrate [27], and humic acid [28]. On the other hand, the fabrication of chitosan–metal oxides has attracted the attention of a lot of scientists owing to their numerous beneficial characteristics, such as chemical stability, a large surface area, and favorable adsorptive characteristics [29]. Magnesium oxide ( $\text{MgO}$ ) [30], titanium oxide ( $\text{TiO}$ ) [31], zinc oxide ( $\text{ZnO}$ ) [32,33], zirconium oxide ( $\text{ZrO}$ ) [34], and copper oxide ( $\text{CuO}$ ) [35] are examples of metal oxides.  $\text{ZrO}$  was selected for this study owing to its strong affinity for anions [36].

The separation of the adsorbents is another issue of concern since the usual separation procedures result in the loss of the adsorbents as well as possible dangers to the environment [37,38]. Magnetite ( $\text{Fe}_3\text{O}_4$ ) is one of the most magnetic particles that can be used in the manufacture of magnetic adsorbents for water purification because of its biodegradability, thermal stability, and large surface area [39,40]. The use of the crosslinking method to combine magnetite, zeolite,  $\text{ZrO}$ , and chitosan is a viable strategy. This is because the magnetic particles allow for easy separation when subjected to an external magnetic field, while the chitosan, zeolite, and  $\text{ZrO}$  provide many adsorption sites [41]. Therefore, the amalgamation of chitosan/zeolite/ $\text{ZrO}$ , and  $\text{Fe}_3\text{O}_4$  (CS-ZL/ $\text{ZrO}/\text{Fe}_3\text{O}_4$ ) may result in the development of novel composite materials with multifunctional constituents.

This study synthesized CS-ZL/ $\text{ZrO}/\text{Fe}_3\text{O}_4$  with the target of using it as a novel adsorbent for  $\text{PO}_4^{3-}$  removal from water. The response surface methodology (RSM) with the Box–Behnken design (BBD) optimization strategy was used to acquire insight into the effect of process factors such as pH, adsorbent dosage, temperature, and time to achieve the maximal adsorptive removal of  $\text{PO}_4^{3-}$ . This process was performed to obtain the highest  $\text{PO}_4^{3-}$  adsorptive removal. The adsorption isotherms and kinetic models were also calculated to figure out the adsorption mechanism.

## 2. Results and Discussion

### 2.1. Characterization of CS-ZL/ $\text{ZrO}/\text{Fe}_3\text{O}_4$

The experimental results of BBD are listed in Table 1. It can be concluded that a pH of 2 offers the best conditions for  $\text{PO}_4^{3-}$  removal. The  $\text{pH}_{\text{ZPC}}$  findings revealed that, at a pH of 2, the surface of CS-ZL/ $\text{ZrO}/\text{Fe}_3\text{O}_4$  had a positive charge ( $\text{pH} < \text{pH}_{\text{ZPC}}$ ) (Figure 1a). This might indicate the protonation of the  $-\text{NH}_2$  groups to  $-\text{NH}_3^+$  groups on the surface. These

attract negatively charged  $\text{H}_2\text{PO}_4^-$  ions to CS-ZL/ZrO/Fe $_3\text{O}_4$ , resulting in the construction of a surface complex between  $\text{PO}_4^{3-}$  ions and CS-ZL/ZrO/Fe $_3\text{O}_4$ . This study was similar to that reported by [42,43], which used SCBC-La and leftover coal, respectively, for  $\text{PO}_4^{3-}$  removal under acidic conditions. The other possible reaction that could occur is shown in Equation (1).



**Table 1.** Experimental data results from 4 factors of BBD for  $\text{PO}_4^{3-}$  removal onto CS-ZL/ZrO/Fe $_3\text{O}_4$ .

Run	pH	Dosage	Temperature	Time	% Removal
1	2	0.02	45	35	58.95
2	10	0.02	45	35	51.75
3	2	0.10	45	35	72.77
4	10	0.10	45	35	54.54
5	7	0.06	30	10	61.83
6	7	0.06	60	10	56.68
7	7	0.06	30	60	64.95
8	7	0.06	60	60	64.94
9	2	0.06	45	10	59.09
10	10	0.06	45	10	54.34
11	2	0.06	45	60	72.75
12	10	0.06	45	60	59.57
13	7	0.02	30	35	56.02
14	7	0.10	30	35	61.46
15	7	0.02	60	35	56.69
16	7	0.10	60	35	59.69
17	2	0.06	30	35	66.84
18	10	0.06	30	35	60.16
19	2	0.06	60	35	64.70
20	10	0.06	60	35	55.08
21	7	0.02	45	10	54.40
22	7	0.10	45	10	58.87
23	7	0.02	45	60	56.72
24	7	0.10	45	60	69.58
25	7	0.06	45	35	53.48
26	7	0.06	45	35	55.47
27	7	0.06	45	35	53.47

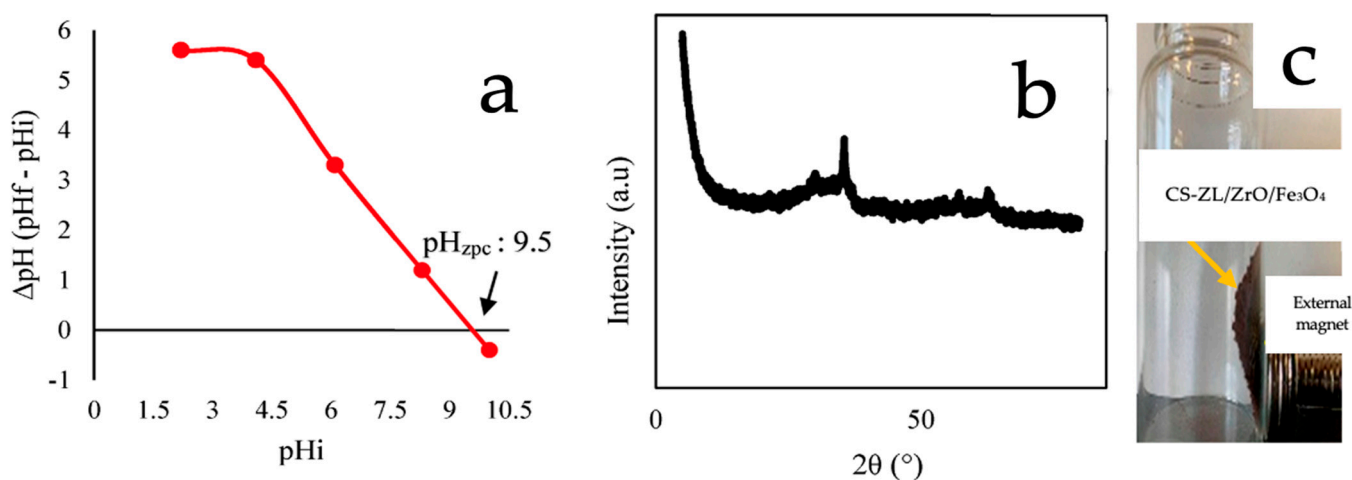


**Figure 1.** (a)  $\text{pH}_{\text{zpc}}$  of CS-ZL/ZrO/Fe $_3\text{O}_4$ , (b) XRD spectra of CS-ZL/ZrO/Fe $_3\text{O}_4$ , and (c) photograph of CS-ZL/ZrO/Fe $_3\text{O}_4$  (taken by phone).

Table 2 summarizes the physical characteristics of these adsorbents. The results show that the BET-specific surface area was  $88.1 \text{ m}^2/\text{g}$ , with a pore volume of  $0.572 \text{ mL/g}$ , an

average diameter of 43.9  $\mu\text{m}$ , and a porosity of 59%. These parameters show that the adsorbent had a substantial surface area for the adsorption of  $\text{PO}_4^{3-}$  ions.

**Table 2.** Physical properties of the adsorbent.

Specific Surface Area	Value
BET-specific surface area ( $\text{m}^2/\text{g}$ )	88.1
Pore volume ( $\text{mL}/\text{g}$ )	0.572
Average diameter ( $\mu\text{m}$ )	43.9
Porosity (%)	59

Figure 1b shows the XRD data used to verify the crystalline structure of the composite material. The XRD pattern shows a huge hump around  $2\theta = 21.22$ , which is a chitosan-specific peak [20]. Furthermore, the sharp peaks at 30.11, 35.49, 43.21 are mostly composed of crystalline phases, such as quartz, hematite, and alumina, which are all formed from zeolite- and zirconium-based materials. Magnetite corresponds to the peaks at 53.52, 57.08, and 62.78 [44]. Figure 1c shows a photograph of CS-ZL/ZrO/Fe<sub>3</sub>O<sub>4</sub>. It can be seen that the adsorbent is attached to the external magnet.

The SEM-EDS characterization of CS-ZL/ZrO/Fe<sub>3</sub>O<sub>4</sub> was carried out to explore the surface properties and chemical components of the material. Figure 2 and Table 3 compare the SEM images and EDS data before and after  $\text{PO}_4^{3-}$  adsorption. Before adsorption, the surface morphology of the adsorbent was sticky, rough, and porous. The surface became smooth and compact after  $\text{PO}_4^{3-}$  adsorption, and this indicates that  $\text{PO}_4^{3-}$  ions were trapped on the adsorbent surface. The primary objective of the EDS data analysis was to identify the components of the adsorbent materials. The weight percentages of Zr and Fe were the highest at 50.68 and 38.92%, respectively. The N value was derived from the chitosan materials [45–47]. Al, Si, and Fe were derived from zeolite and magnetite, respectively. Furthermore, the presence of P after the adsorption process indicates that  $\text{PO}_4^{3-}$  was successfully adsorbed.

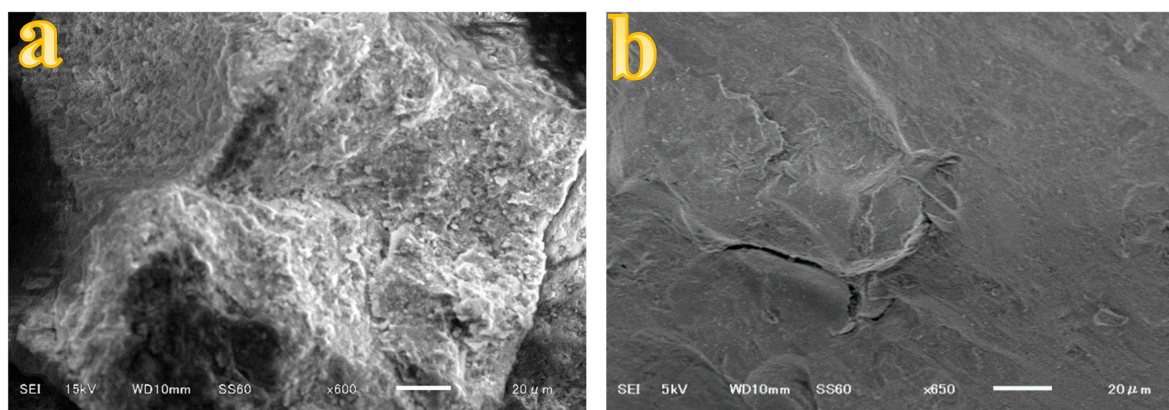


**Figure 2.** SEM images before (a), and after (b)  $\text{PO}_4^{3-}$  adsorption.

**Table 3.** EDS data before and after  $\text{PO}_4^{3-}$  adsorption.

Element	Weight %		Atomic %	
	Before	After	Before	After
N	3.27	2.06	13.43	7.66
Al	0.78	0.93	1.65	1.79
Si	6.35	1.70	12.98	3.15
Fe	38.92	56.39	40.03	52.69
Zr	50.68	27.76	31.91	15.88
P		11.17		18.82

Figure 3 shows the functional groups in CS-ZL/ZrO/Fe<sub>3</sub>O<sub>4</sub> before and after PO<sub>4</sub><sup>3-</sup> adsorption through an FTIR-ATR analysis. A CS-ZL/ZrO/Fe<sub>3</sub>O<sub>4</sub> band was detected following PO<sub>4</sub><sup>3-</sup> adsorption from 3326 cm<sup>-1</sup> to 3320 cm<sup>-1</sup>. This shows that PO<sub>4</sub><sup>3-</sup> ions interact with the stretching vibrations of hydrogen and amine in chitosan [48]. After PO<sub>4</sub><sup>3-</sup> adsorption, a decrease in the peak from 1634 to 1627 cm<sup>-1</sup> was observed, which is associated with carboxyl groups (-COOCH<sub>3</sub>) [49]. An increased peak and a more curved and newer peak appeared after PO<sub>4</sub><sup>3-</sup> adsorption from 951 to 1006 cm<sup>-1</sup> and at 2161 cm<sup>-1</sup>, which were assigned to Si-O-Al, Fe-O-Si, or Zr-O-Fe and CN stretching, respectively. This indicated a strong interaction with PO<sub>4</sub><sup>3-</sup> ions.

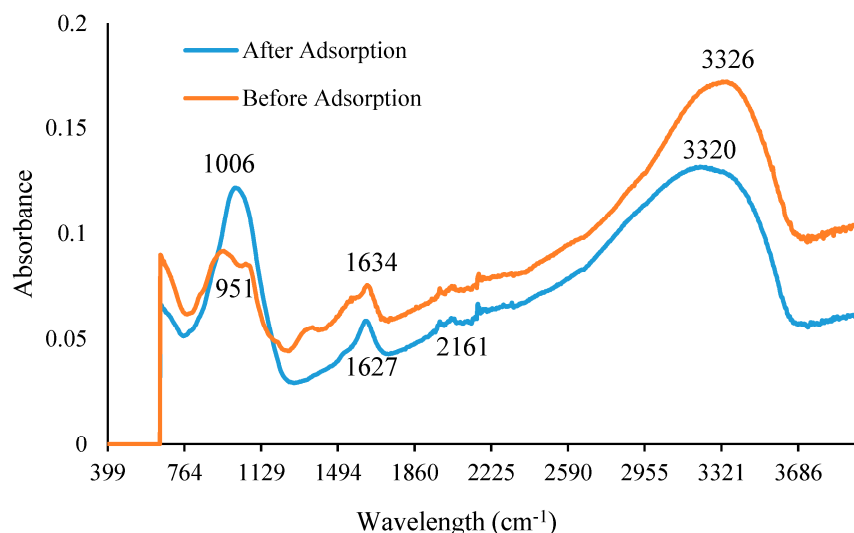


**Figure 3.** FTIR-ATR before, and after PO<sub>4</sub><sup>3-</sup> adsorption.

## 2.2. Mechanical Stability

The mechanical stability of the CS-ZL/ZrO/Fe<sub>3</sub>O<sub>4</sub> composite was determined through the percentage of the initial mass that was preserved after drying. Figure 4a shows that increasing the concentration of the solution led to a higher WR%. Compared to the HCl-containing solution, the H<sub>2</sub>SO<sub>4</sub>-containing solution exhibited a higher WR%. Consequently, the crystalline structure of CS-ZL/ZrO/Fe<sub>3</sub>O<sub>4</sub> was deformed, indicating that H<sub>2</sub>SO<sub>4</sub> had significant contact with the chitosan group. Figure 4b shows the IR spectra after treatment. The positions of the peaks were consistent for all the samples. According to [50], the broad band visible at 3176–3345 cm<sup>-1</sup> is assigned to the -NH<sub>2</sub> groups changing to -NH<sub>3</sub><sup>+</sup> groups. The peaks between 1611 and 1630 cm<sup>-1</sup>, which were ascribed to the carboxyl (-COOCH<sub>3</sub>) and -NH<sub>2</sub> groups, were generated through H<sup>+</sup> generation by HCl and H<sub>2</sub>SO<sub>4</sub>. The peak shifted to 1068 cm<sup>-1</sup>, and expansion occurred when treated with 0.1 M H<sub>2</sub>SO<sub>4</sub>. SO<sub>4</sub><sup>2-</sup> ions have been shown to be associated with Si, Al, Fe, and Zr [51]. According to these results, the physical and chemical characteristics of the CS-ZL/ZrO/Fe<sub>3</sub>O<sub>4</sub> composites did not change significantly.

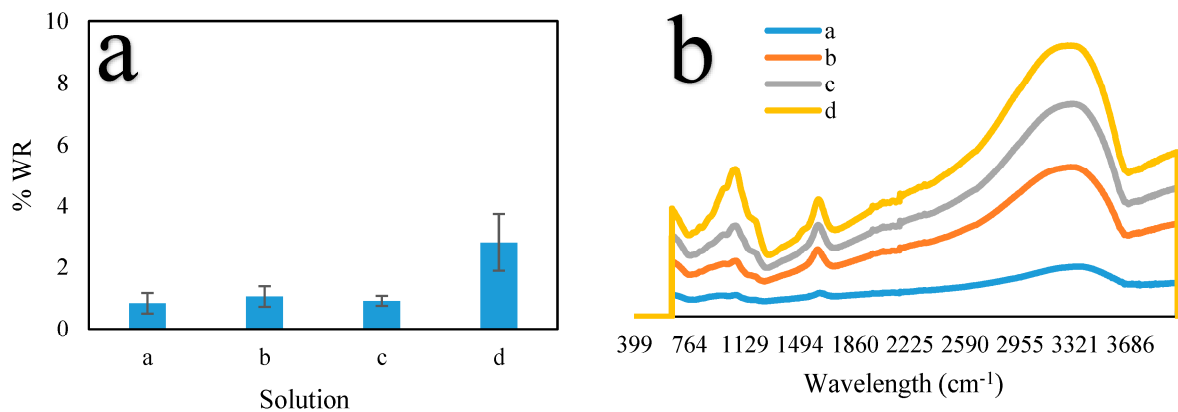


**Figure 4.** WR of CS-ZL/ZrO/Fe<sub>3</sub>O<sub>4</sub>. (a) Percentage WR, and (b) FTIR-ATR of CS-ZL/ZrO/Fe<sub>3</sub>O<sub>4</sub> after treatment. Solution a (0.01 M HCl), b (0.1 M HCl), c (0.01 M H<sub>2</sub>SO<sub>4</sub>), and d (0.1 M H<sub>2</sub>SO<sub>4</sub>). Standard deviation (error bars).

### 2.3. ANOVA and Equations for Fitting Empirical Models

Table 4 shows the results of the statistical analysis, using the ANOVA test to evaluate the relationship between the input effective variables (A, B, C, and D) and their responses (Y). Table 4 shows that the F-value of the quadratic model was 16.68 and that the *p*-value was <0.0001, indicating that this model was significant. Models A, B, D, A<sup>2</sup>, C<sup>2</sup>, D<sup>2</sup>, A × B, A × D, and C × D, marked with an asterisk (\*), were found to be significant parameters of the model. The statistical variables obtained from the ANOVA test (Equation (2)) provide a full quadratic regression model for PO<sub>4</sub><sup>3-</sup> removal (%).

$$\text{PO}_4^{3-} \text{ removal (\%)} = 99.2 - 1.72 A + 63 B - 1.478 C - 0.472 D + 0.2333 A^2 + 840 B^2 + 0.01575 C^2 + 0.00661 D^2 - 17.23 A*B - 0.0123A*C - 0.02107 A*D - 1.02 B*C + 2.098 B*D + 0.00343 C*D \quad (2)$$

**Table 4.** ANOVA results for PO<sub>4</sub><sup>3-</sup> removal.

Source	DF	Sum of Squares	Mean of Squares	F-Value	<i>p</i> -Value	Remarks
Model	14	839.751	59.982	16.68	<0.0001 *	Significant
A	1	296.610	296.610	51.8093	<0.0001 *	
B	1	149.672	149.672	12.5582	<0.0001 *	
C	1	15.143	15.143	1.2835	0.063	
D	1	156.241	156.241	0.6342	<0.0001 *	
A <sup>2</sup>	1	74.285	74.285	12.8151	0.001 *	
B <sup>2</sup>	1	9.642	9.642	1.4722	0.127	
C <sup>2</sup>	1	67.008	67.008	7.1279	0.001 *	
D <sup>2</sup>	1	90.952	90.952	1.9374	<0.0001 *	
A × B	1	30.415	30.415	4.2734	0.013 *	
A × C	1	2.161	2.161	0.3036	0.453	
A × D	1	17.766	17.766	8.2118	0.046 *	
B × C	1	1.488	1.488	0.2091	0.532	
B × D	1	17.598	17.598	0.0540	0.047 *	
C × D	1	6.605	6.605	1.84	0.200	
Error	12	43.157	3.596			
Lack-of-Fit	10	40.504	4.050	3.05	0.272	
Pure Error	2	2.653	1.3267			
Total	26	882.908				
R <sup>2</sup>		95.11				
R <sup>2</sup> adj		89.41				

\* Significant.

The coefficients in the equation with positive and negative signs describe the additive and multiplicative effects of the variables on the response. The “Lack of Fit” was determined by comparing the residual error to the pure error in close proximity to the repeatedly

designed points.  $F = 3.05$  and  $p = 0.272$  for the “Lack of Fit” revealed that it was not significant for the model ( $p < 0.05$ ). It can be assumed that the model was adequately fitted and that there was no lack of fit.

The  $R^2$  value of the calculated second-order response model was 95.11, which is also known as the coefficient of determination. Consequently, it can be applied to reliably calculate the response at any given parameter level regardless of their values. In addition, a regression model was used to calculate the standardized influence of the independent factors on  $\text{PO}_4^{3-}$  removal. A response surface plot was generated to investigate the influence of two components at initial the  $\text{PO}_4^{3-}$  concentration of 20 mg/L (Figure 5). This plot was used to determine the standardized effects of all the independent variables. A surface plot is an easier way to display the response behavior that occurs when two parameters are simultaneously altered at the same time. It is more beneficial to select the quantity of various ingredients to obtain the desired response. Figure 5a displays a Pareto chart that compares the relative magnitude and the corresponding main, square, and interaction effects of the selected variables. The square effects of all four factors were found to be very significant ( $p \leq 0.05$ ) in addition to the main effects of the factors, which were also found to be highly significant ( $p \leq 0.05$ ). The ANOVA results reported in Table 4 led to the same conclusions.  $\text{PO}_4^{3-}$  removal continuously increased in response to the pH, adsorbent dosage, and time. Figure 5b,c show that pH is a key factor in the removal of  $\text{PO}_4^{3-}$ , and Figure 5d shows that increasing the contact time increases the percentage removal.

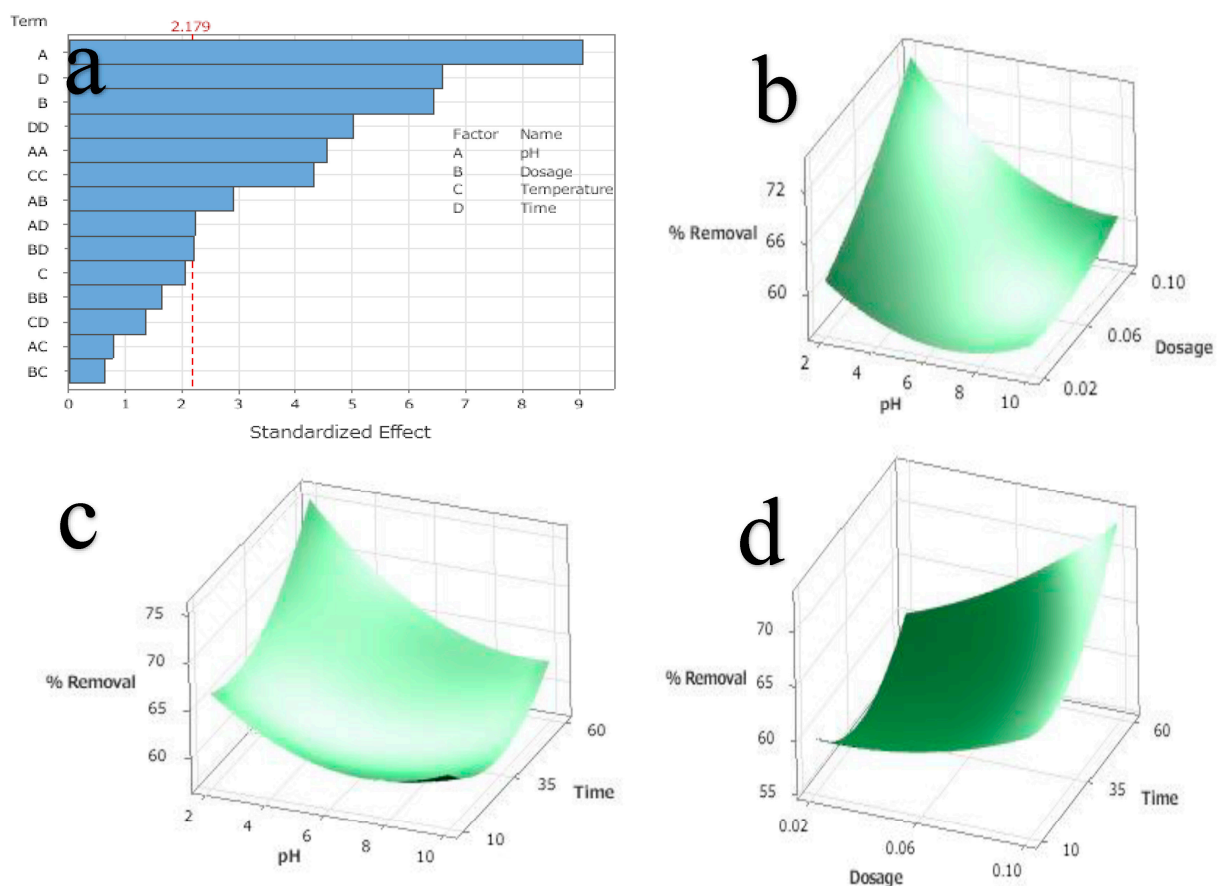


**Figure 5.** (a) Pareto chart for the standardized effect of various factors on  $\text{PO}_4^{3-}$  removal by adsorbent, (b) pH and dosage of adsorbent response surface's effect on  $\text{PO}_4^{3-}$  removal (%), (c) pH and time response surface's effect on  $\text{PO}_4^{3-}$  removal (%), and (d) pH and dosage of adsorbent and time response surface's effect on  $\text{PO}_4^{3-}$  removal (%).

### 2.4. Initial Concentration and Isotherm Studies

The effects of the initial  $\text{PO}_4^{3-}$  concentrations ranging from 20 to 500 mg/L, 0.06 g of adsorbent (CS-ZL/ZrO/Fe<sub>3</sub>O<sub>4</sub>), and pH (2.0) were investigated. Figure 6 shows that the  $\text{PO}_4^{3-}$  adsorption capacity rose from 30.64 to 682.31 mg/g; however, the percentage of  $\text{PO}_4^{3-}$  removal decreased from 91.91% to 81.88%. The adsorption capacity increased with the concentration because the total number of molecules increased. Consequently, the mass transfer resistance of adsorbate decreased. As a result, the percentage of removal decreased [52].

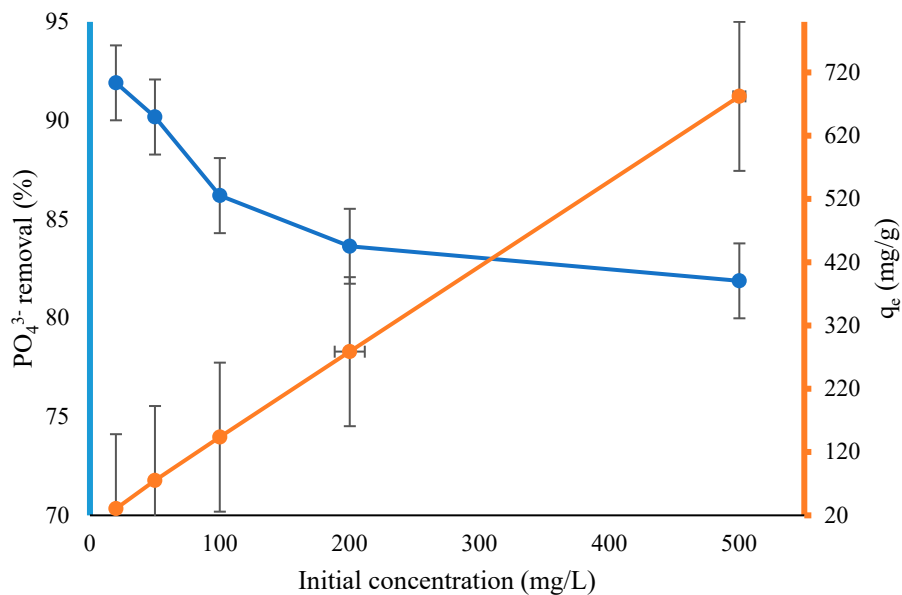


**Figure 6.** Effect of initial concentration on  $\text{PO}_4^{3-}$  removal onto CS-ZL/ZrO/Fe<sub>3</sub>O<sub>4</sub>. Standard deviation (error bars).

Adsorption isotherms are necessary to assess the capabilities of an adsorbent and the interactions between an adsorbate (a solution containing  $\text{PO}_4^{3-}$  ions) and an adsorbent (CS-ZL/ZrO/Fe<sub>3</sub>O<sub>4</sub>). The acquired isotherm parameters can be used to conduct an accurate analysis while constructing an effective adsorption system. Both the equilibrium concentration and the adsorption capacity were estimated. The Langmuir model describes the monolayer adsorption processes at the designated homogenous surfaces on the adsorbent (Equation (3)). The essential property of the Langmuir model can be described as a dimensionless constant also known as the separation factor ( $R_L$ ), which is shown in Equation (4). By contrast, the Freundlich model is based on heterogeneous surfaces and multilayer sorption (Equation (5)). This is a linear equation, which is shown as follows:

$$C_e/q_e = \left(\frac{C_e}{q_{\max}}\right) + 1/(K_1 q_{\max}) \tag{3}$$

$$R_L = \left(\frac{1}{1 + bC_o}\right) \tag{4}$$

$$\ln q = \ln K_f + \frac{1}{n} \times \ln C_e \tag{5}$$

$q_e$  (mg/g) is the adsorption capacity;  $K_1$  (L/mg) is the equilibrium constant of adsorption;  $q_{\max}$  (mg/g) is the maximal adsorption capacity;  $C_e$  (mg/L) is the equilibrium concentration;  $C_o$  (mg/L) is the initial concentration;  $R_L$  is the separation factor;  $0 < R_L$  is favorable;  $R_L > 1$  is unfavorable;  $R_L = 1$  is linear; and  $K_f$  (mg/g) and  $1/n$  are the adsorption capacity and the intensity of adsorption, respectively.

Figure 7 shows the isotherm model curves, and Table 5 shows the fitting results corresponding to these curves. The Freundlich model's linear correlation coefficient ( $R^2$ ) was 0.9970, indicating that it provided the best fit compared to the other models. More importantly, the Langmuir and Freundlich parameters, known as  $R_L$  and  $1/n$ , indicate that the  $\text{PO}_4^{3-}$  ion has a type of  $<1$ . According to these data, the  $\text{PO}_4^{3-}$  adsorption method is favorable.

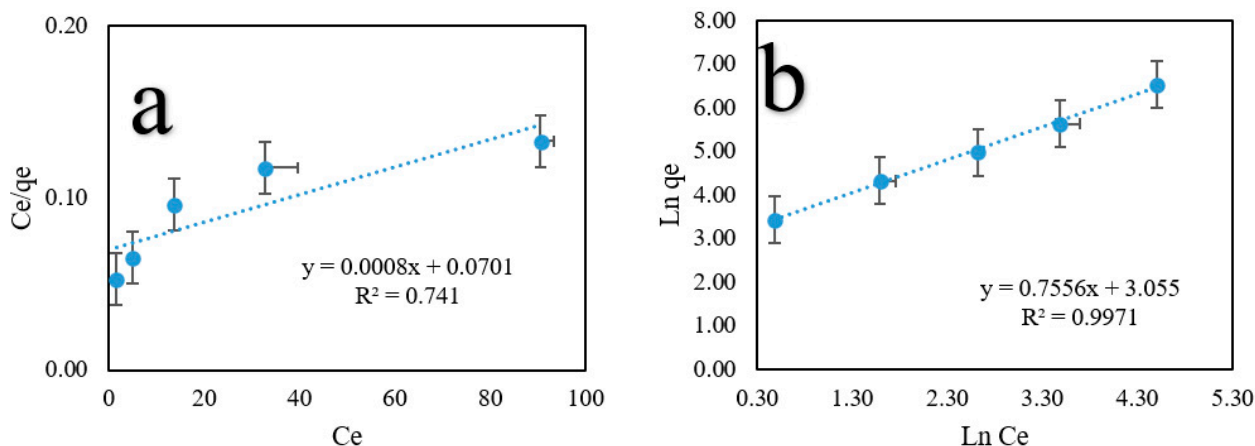


**Figure 7.** Linear curves of  $\text{PO}_4^{3-}$  adsorption isotherm models. (a) Langmuir, and (b) Freundlich models. Standard deviation (error bars).

**Table 5.** Isotherm model parameters for  $\text{PO}_4^{3-}$  removal onto CS-ZL/ZrO/Fe<sub>3</sub>O<sub>4</sub>.

Isotherms	Parameters	Value
Langmuir	$q_{\max}$	1259.79
	$K_L$	14.27
	$R^2$	0.7409
	$R_L$	0.0007
Freundlich	$K_f$	1135.07
	$1/n$	0.7555
	$R^2$	0.9970

### 2.5. Adsorption Kinetic Studies

This study investigated the influence of the contact time (35–2880 min) on  $\text{PO}_4^{3-}$  adsorption at 30 °C. Figure 8 shows that the percentage of  $\text{PO}_4^{3-}$  removal and the capacity for adsorption increased rapidly from 35 to 60 min and then gradually increased up to 90 min. This is because the adsorbent includes carboxyl, amine, hydrogen, and magnetite groups, all of which cause the adsorbent surface to become active and trap  $\text{PO}_4^{3-}$  ions. Subsequently, the adsorption capacity decreased and increased, resulting in fast/slow  $\text{PO}_4^{3-}$  adsorption, and it finally reached equilibrium at 1440 min, with an adsorption capacity and percent removal of 732.56 mg/g and 87.91%, respectively.

Adsorption kinetic studies are important because they deliver information on the adsorption mechanism, which is necessary to assess the effectiveness of the process [53]. Two kinetic models were used in this study: pseudo-first-order (PFO) (Equation (6)) and pseudo-second-order (PSO) (Equation (7)) models were investigated. The linear form can be obtained by calculating the following equation.

$$\text{Log}(q_e - q_t) = \text{log } q_e - K_1 t \quad (6)$$

$$t/q_t = 1/(K_2 q_e^2) + t/q_e \quad (7)$$

where  $k_1$  ( $\text{min}^{-1}$ ) is the rate constant of the PFO model,  $t$  (min) is the time, and a linear plot of  $\log t$  against  $\log (q_e - q_t)$  and  $t$  against  $t/q_t$  was used to determine  $K_1$  and  $K_2$  from the slope of the linear plots, respectively.

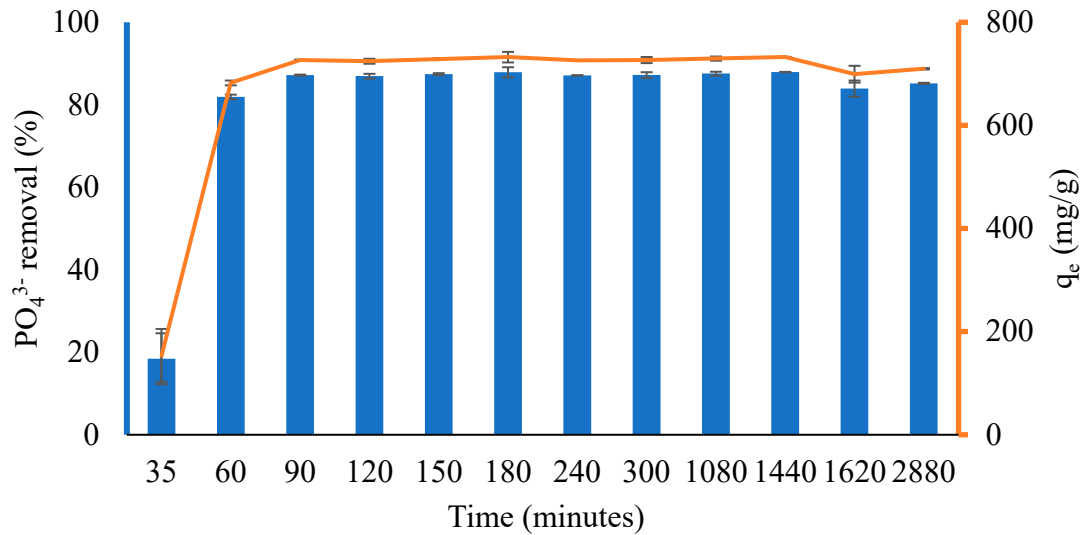


**Figure 8.** The effect of contact time on  $\text{PO}_4^{3-}$  removal onto CS-ZL/ZrO/Fe<sub>3</sub>O<sub>4</sub>. Standard deviation (error bars).

Figure 9 shows the fitting curves for the kinetic models, and Table 6 lists the fitting results corresponding to those curves. The findings confirm that the PSO model provided better results than the PFO model in terms of the linear correlation coefficient  $R^2$  value (0.9979). These findings imply that chemical processes control the adsorption rate.

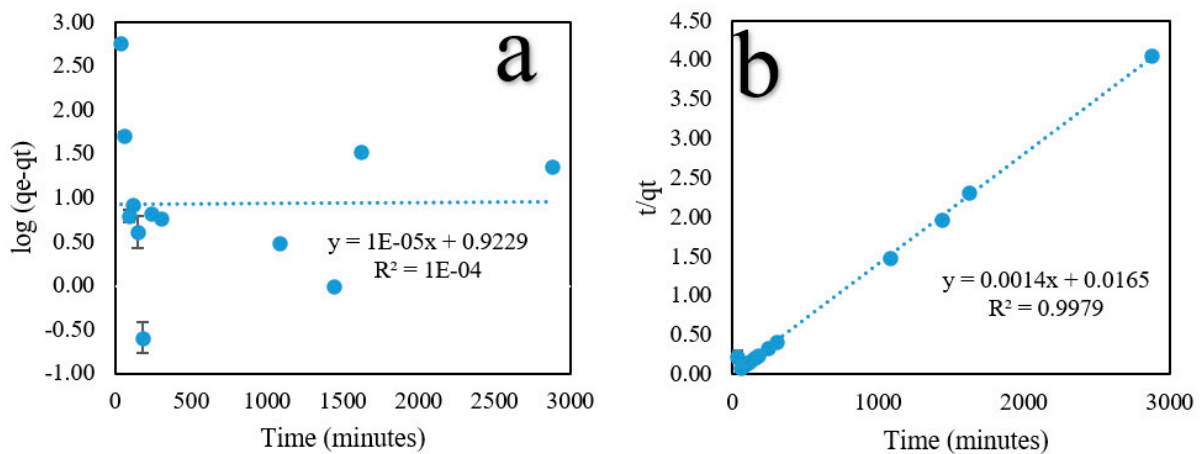


**Figure 9.** Linear curves of  $\text{PO}_4^{3-}$  adsorption kinetic studies. (a) Pseudo-first-order (PFO) and (b) pseudo-second-order (PSO) models. Standard deviation (error bars).

**Table 6.** Kinetic model parameters for  $\text{PO}_4^{3-}$  removal onto CS-ZL/ZrO/Fe<sub>3</sub>O<sub>4</sub>.

Kinetics	Parameters	Value
PFO	$q_e$	2.5165
	$K_1$	$1.42857 \times 10^{-6}$
	$R^2$	$1.00 \times 10^{-4}$
PSO	$q_e$	510,204.1
	$K_2$	0.000119
	$R^2$	0.9979

### 2.6. Effect of Anions and Cations on $\text{PO}_4^{3-}$ Removal onto CS-ZL/ZrO/Fe<sub>3</sub>O<sub>4</sub>

Wastewater contains various substances, including anions and cations, which can affect the adsorption process [54]; it is essential to investigate the effect of ionic strength in an aqueous solution. This is because wastewater is made up of numerous components that might be found together. Figure 10 depicts the effect of different anions and cations on the  $\text{PO}_4^{3-}$  adsorption capacity of CS-ZL/ZrO/Fe<sub>3</sub>O<sub>4</sub>. The experimental data indicate that there was no significant influence on  $\text{PO}_4^{3-}$  removal. It revealed that the fabrication of CS-ZL/ZrO/Fe<sub>3</sub>O<sub>4</sub> was effective in eliminating  $\text{PO}_4^{3-}$  from water.

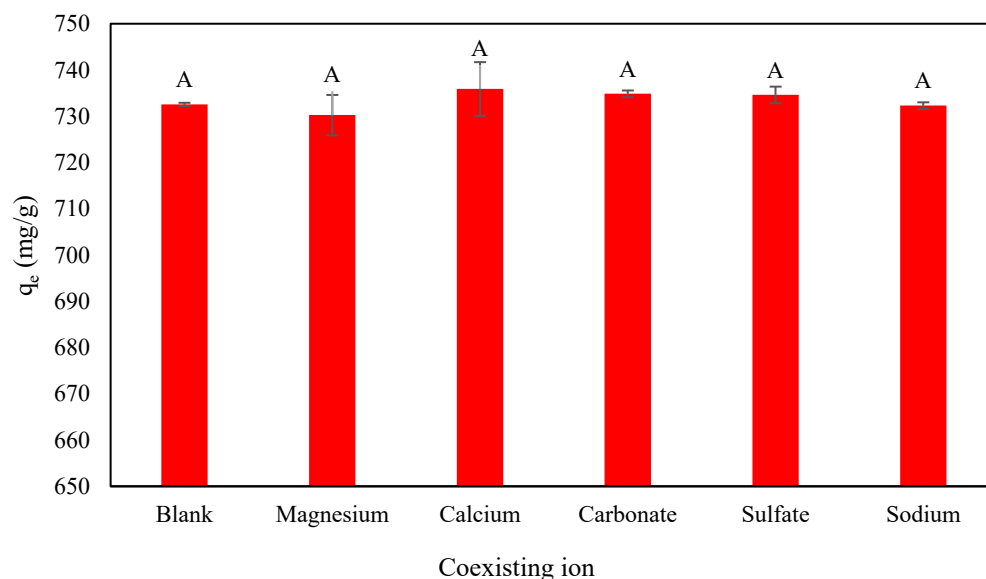


**Figure 10.** The effect of coexisting ions on  $\text{PO}_4^{3-}$  removal onto CS-ZL/ZrO/Fe<sub>3</sub>O<sub>4</sub>. Standard deviation (error bars). A: no significant effect ( $p \leq 0.05$ ).

### 2.7. Desorption Studies

Figure 11a shows the desorption percentage of  $\text{PO}_4^{3-}$  at different NaOH concentrations from 0.01 M to 1 M for 30 min at 30 °C. The results indicate that increasing the concentration increased the desorption percentage to 95.77%. Then, subsequent experiment at different contact times, from 30 to 150 min, using 1 M NaOH (Figure 11b). The desorption percentage increased and then decreased up to 150 min, which is similar to the results of the adsorption studies. The highest desorption percentage was observed after 30 min. The desorption mechanism may cause the hydroxide ions ( $\text{OH}^-$ ) in the sodium hydroxide solution to react with the CS-ZL/ZrO/Fe<sub>3</sub>O<sub>4</sub>-P surface and replace the  $\text{PO}_4^{3-}$  groups, resulting in the release of  $\text{PO}_4^{3-}$  into the liquid solution (Equation (8)). The reusability studies of  $\text{PO}_4^{3-}$  adsorption onto CS-ZL/ZrO/Fe<sub>3</sub>O<sub>4</sub> showed good performance for three cycles (Figure 11c).



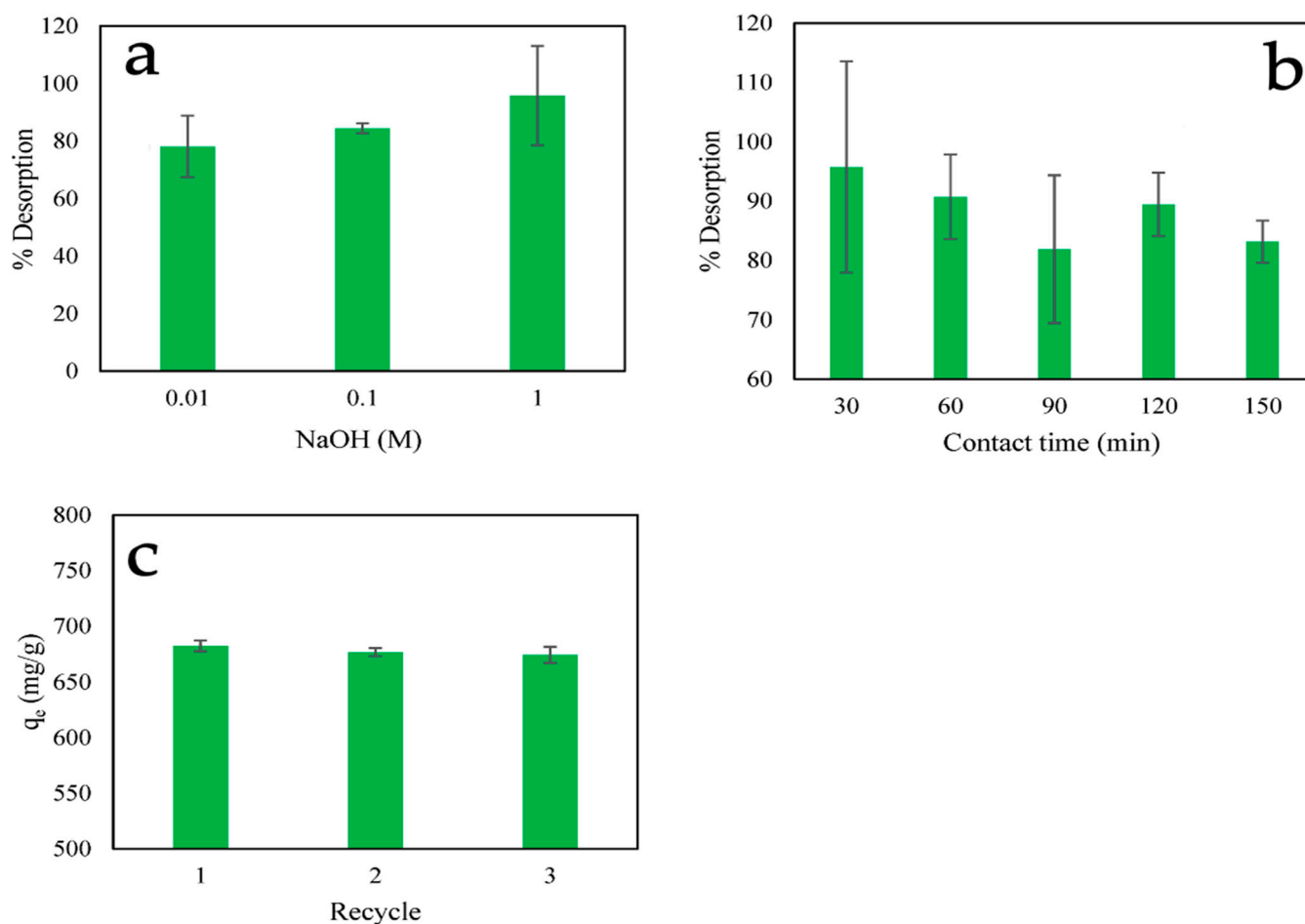


**Figure 11.** The percentage of desorption. (a) Different NaOH concentrations and (b) different contact times using 1 M NaOH, and (c) in recycle studies on  $\text{PO}_4^{3-}$  adsorption capacity. Standard deviation (error bars).

### 2.8. Adsorption Performance Comparison

Table 7 compares the equilibrium and maximum adsorption capacity of CS-ZL/ZrO/Fe<sub>3</sub>O<sub>4</sub> with those of various adsorbents. It can be seen that the pH is one of the main factors for  $\text{PO}_4^{3-}$  removal onto the adsorbent, and the surface charge can become either positive or negative over a wide pH range, which influences the interaction between the adsorbent and  $\text{PO}_4^{3-}$  ions. It is clear that the CS-ZL/ZrO/Fe<sub>3</sub>O<sub>4</sub> adsorbent has a higher capacity than the other adsorbents. It is feasible to conclude that these adsorbents are viable alternatives for removing  $\text{PO}_4^{3-}$  from water.

**Table 7.** List comparing  $\text{PO}_4^{3-}$  adsorption amounts.

Adsorbent	pH	$q_e$ (mg/g)	References
Magnetic iron oxide nanoparticles	11	5.03	[1]
Fe-HNT	4	5.46	[18]
Halloysite	4	3.56	[18]
20MMSB	4	121.25	[55]
Amine-functionalized nano magnetic Fe <sub>3</sub> O <sub>4</sub> polymer	3.0	102.04	[56]
MFB-MCs	3.0	487.99	[57]
Fe <sub>3</sub> O <sub>4</sub> @SiO <sub>2</sub> core/shell magnetic nanoparticles	-	27.8	[58]
AgNPs-TAC	3	13.62	[59]

Table 7. Cont.

Adsorbent	pH	q <sub>e</sub> (mg/g)	References
Ce <sub>0.8</sub> Zr <sub>0.2</sub> O <sub>2</sub>	6.2	112.23	[60]
Zr/Al-Mt	5.0	17.2	[61]
PZC 7.3	11	2.41	[62]
Zeolite	11	0.69	[62]
Biochar	11	3.60	[62]
CS-ZL/ZrO/Fe <sub>3</sub> O <sub>4</sub>	2	732.56	Present study

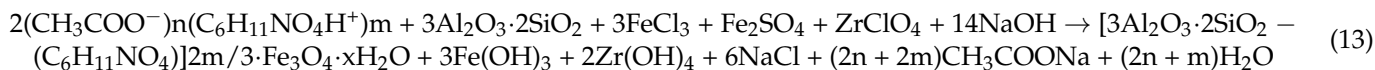
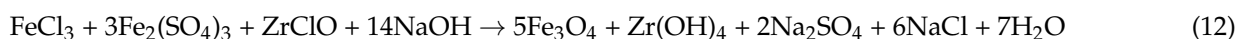
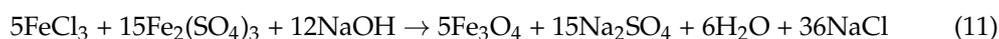
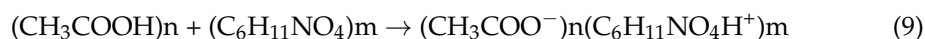
### 3. Materials and Methods

#### 3.1. Materials

Chitosan (CH) (C<sub>6</sub>H<sub>11</sub>NO<sub>4</sub>) with molecular weight of 100,000–300,000 Da was bought from Acros Organics, Belgium. Zeolite (ZL) (Al<sub>2</sub>O<sub>3</sub>·2SiO<sub>2</sub>) was obtained from Tosoh Co. Ltd., Japan. Sodium hydroxide (NaOH), acetic acid (CH<sub>3</sub>COOH), disodium hydrogen phosphate (Na<sub>2</sub>HPO<sub>4</sub>), ferric chloride (FeCl<sub>3</sub>), ferrous sulfate (Fe<sub>2</sub>SO<sub>4</sub>), ammonium molybdate ((NH<sub>4</sub>)<sub>6</sub>Mo<sub>7</sub>O<sub>24</sub>·4H<sub>2</sub>O), antimony potassium tartrate (K<sub>2</sub>Sb<sub>2</sub>(C<sub>4</sub>H<sub>2</sub>O<sub>6</sub>)<sub>2</sub>), ascorbic acid (C<sub>6</sub>H<sub>8</sub>O<sub>6</sub>), hydrochloric acid (HCl), and sulfuric acid (H<sub>2</sub>SO<sub>4</sub>) were bought from Kanto Chemical Co., Inc., Tokyo, Japan. ZrClO was purchased from Fujifilm Wako Chemical, Tokyo, Japan.

#### 3.2. Synthesis of CS-ZL/ZrO/Fe<sub>3</sub>O<sub>4</sub>

CS-ZL/ZrO/Fe<sub>3</sub>O<sub>4</sub> was synthesized through crosslinking method; chitosan (1 g) was dissolved in 100 mL of acetic acid (1%), and the resulting viscous solution was maintained at ambient temperature (25–30 °C) with magnetic stirring for 24 h (Equation (9)). Subsequently, 25 mL of the resulting chitosan solution was mixed with 0.5 g of zeolite and 20 mL of 1 M FeCl<sub>3</sub> + 0.5 M Fe<sub>2</sub>SO<sub>4</sub> + 0.5 M ZrClO. The mixture solution was then heated to 60 °C and was stirred for 1 h. The pH of the solution was adjusted to 10 using 3 M NaOH over 24 h with magnetic stirring at ambient temperature (25–30 °C), and the solution was filtered and washed multiple times with acetone and distilled water (DW) to remove any remaining NaOH. Subsequently, the materials were dried for 48 h in an oven at 60 °C (Equation (13)). The adsorbents are referred to as CS-ZL/ZrO/Fe<sub>3</sub>O<sub>4</sub>.



Following this reaction, the negatively charged surface of the zeolite (Al<sub>2</sub>O<sub>3</sub>·2SiO<sub>2</sub>) may interact with the positively charged chitosan to produce chitosan–aluminosilicate complex. Electrostatic interactions between Fe<sup>3+</sup> and Zr<sup>4+</sup> ions and chitosan are another mechanism by which chitosan combines with metal ions to form chitosan–metal complexes. Fe(OH)<sub>3</sub> and Fe<sub>3</sub>O<sub>4</sub> are formed when Fe<sup>2+</sup> and Fe<sup>3+</sup> ions react with hydroxide ions (OH<sup>−</sup>) from NaOH.

#### 3.3. The Design of the Experiment

Experiments were conducted using response surface methodology (RSM) in combination with Box–Behnken design (BBD), and statistical analysis was performed using Minitab 21.3.1 software. (A) The pH (2–10), (B) dosage (0.02–0.1 g), (C) temperature (30–60 °C),

and (D) contact time (10–60 min) were the independent variables examined in the BBD, with three levels and four parameters (Table 8). In total, 27 different sets of experiments were performed to determine the optimal conditions for  $\text{PO}_4^{3-}$  removal. The data obtained were assessed using an equation for a quadratic polynomial response surface, which was calculated using Equation (14), to identify the relationships between independent variables and response.

$$Y = E_0 + E_1A + E_2B + E_3C + E_4D + E_{11}A^2 + E_{22}B^2 + E_{33}C^2 + E_{12}AB + E_{13}AC + E_{23}BC + \varepsilon \quad (14)$$

**Table 8.** Variables and levels.

Symbol	Factor	Level 1 (− 1)	Level 2 (0)	Level 3 (+ 1)
A	pH	2	7	10
B	Dosage (g)	0.02	0.06	0.10
C	Temperature (°C)	30	45	60
D	Time (min)	10	35	60

The coefficients of the polynomial model are represented as follows:  $E_0$  is constant expression,  $E_1$ – $E_3$  are linear effects,  $E_{11}$ – $E_{33}$  are second-order effects,  $E_{12}$ – $E_{23}$  are interactive effects, and  $\varepsilon$  is error term. An analysis of variance (ANOVA) was performed to calculate the  $F$ - and  $p$ -values of the model to measure its statistical significance and appropriateness. The statistical significance of the model is shown through the model's  $F$ -value and  $p$ -value, and a lack-of-fit study of the proposed model was executed using Minitab 21.3.1 software. In addition, a 3D response surface plot and Pareto chart of standardized effects were developed to figure out the cooperative quantitative impact of the independent variables on the response and overall value of the model [63].

### 3.4. Batch Adsorption Study and Response Determination ( $\text{PO}_4^{3-}$ Removal %)

To evaluate the efficiency of  $\text{PO}_4^{3-}$  removal, batch adsorption approach was used in this study. In total, 100 mL of  $\text{PO}_4^{3-}$  (20 mg/L) was placed in a 300 mL conical flask. After the adsorption procedure was completed, external magnetite was placed in the conical flask to separate the adsorbent and adsorbate.  $\text{PO}_4^{3-}$  removal was calculated using Equation (15).

$$\text{PO}_4^{3-} \text{ removal \%} = \frac{C_0 - C_e}{C_0} \times 100 \quad (15)$$

where  $C_0$  and  $C_e$  are the initial and equilibrium  $\text{PO}_4^{3-}$  concentrations (mg/L), respectively.

The data from run 17 of the BBD were used for subsequent experiments (isotherm and kinetic models). However, 30 min was not used because the results were far from equilibrium. The amount of  $\text{PO}_4^{3-}$  adsorbed was determined using Equation (16).

$$q_e = \frac{C_0 - C_e}{W} \times V \quad (16)$$

where  $q_e$  (mg/g) is the adsorption capacity,  $W$  (g) is the amount of CS-ZL/ZrO/Fe<sub>3</sub>O<sub>4</sub>, and  $V$  (L) is the volume of adsorbate ( $\text{PO}_4^{3-}$  solution).

### 3.5. Adsorption Isotherm Studies

The isotherm model was studied with  $\text{PO}_4^{3-}$  solutions ranging from 20 mg/L to 500 mg/L with pH of 2. These examinations were performed for 60 min at 30 °C, and adsorbent dosage of 0.06 g was placed in the flask. In this work, Langmuir and Freundlich models were used to assess  $\text{PO}_4^{3-}$  adsorption onto CS-ZL/ZrO/Fe<sub>3</sub>O<sub>4</sub> [64].

### 3.6. Adsorption Kinetic Studies

Pseudo-first-order (PFO) and pseudo-second-order (PSO) models were used to investigate the model of adsorption kinetics. The following parameters were used in the

experiment: an adsorption temperature of 30 °C, an initial  $\text{PO}_4^{3-}$  concentration of 500 mg/L at pH of 2, an adsorbent dosage of 0.06 g, and contact time ranging from 35 to 2880 min.

### 3.7. Influence of Coexisting Ionic Strength

The experiment was conducted under optimum conditions with a dosage of 0.06 g, an initial  $\text{PO}_4^{3-}$  concentration of 500 mg/L, and a contact time of 1440 min at 30 °C. The coexisting ion was prepared with cationic and anionic ions at a concentration of 20 mg/L ( $\text{Mg}^{2+}$ ,  $\text{Ca}^{2+}$ ,  $\text{CO}_3^{2-}$ ,  $\text{SO}_4^{-}$ , and  $\text{Na}^+$ ).

### 3.8. Desorption and Reusability Studies

In most practical applications, it is essential to employ adsorbents with high level of reusability. NaOH was chosen as desorbing agent to release  $\text{PO}_4^{3-}$  ion from CS-ZL/ZrO/Fe<sub>3</sub>O<sub>4</sub>. Firstly, 0.06 g of CS-ZL/ZrO/Fe<sub>3</sub>O<sub>4</sub> was loaded with 500 mg/L of  $\text{PO}_4^{3-}$  ion at pH of 2.0, which was called CS-ZL/ZrO/Fe<sub>3</sub>O<sub>4</sub>-P. Then, 0.01 g of CS-ZL/ZrO/Fe<sub>3</sub>O<sub>4</sub>-P was dispersed in 60 mL of NaOH at 30 °C. The desorption capacity and desorption percentage are shown in Equations (17) and (18), respectively. Reusability was assessed using the same treatment as described above.

$$q_{\text{des}} = \frac{C}{W} \times V \quad (17)$$

$$\% \text{ Desorption} = \frac{q_{\text{des}}}{q_e} \times 100 \quad (18)$$

where  $q_{\text{des}}$  (mg/g) is the desorption capacity;  $C$  (mg/L) is the  $\text{PO}_4^{3-}$  concentration of desorption; % Desorption (%) is the percentage desorption; and  $W$ ,  $V$ , and  $q_e$  are the same as above.

### 3.9. $\text{PO}_4^{3-}$ Measurements

$\text{PO}_4^{3-}$  ions were measured using the molybdate blue method. A total of 12 g of  $(\text{NH}_4)_6\text{Mo}_7\text{O}_{24} \cdot 4\text{H}_2\text{O}$  was mixed with 100 mL of DW.  $\text{K}_2\text{Sb}_2(\text{C}_4\text{H}_2\text{O}_6)_2$  (0.277 g) was added followed by 140 mL of 18 M  $\text{H}_2\text{SO}_4$ . Afterward, it was adjusted to 1 L with distilled water (solution A). A total of 1.06 g of  $\text{C}_6\text{H}_8\text{O}_6$  was added to and mixed with 100 mL of solution A, 25 mL of 4 N  $\text{H}_2\text{SO}_4$  was added, and the solution was adjusted to 1 L with DW (solution B). Note: This solution must be prepared in every experiment. The procedure for the mixed solution was as follows: 2 mL of liquid sample/standard was mixed with 10 mL of solution B. Afterwards, we waited for 30 min and then analyzed the solution using a UV-Vis spectrophotometer (Jasco V-530) at a wavelength of 693 nm. A standard curve for  $\text{PO}_4^{3-}$  was constructed using  $\text{Na}_2\text{HPO}_4$ .

### 3.10. Mechanical Stability

The mechanical stability of the CS-ZL/ZrO/Fe<sub>3</sub>O<sub>4</sub> composite was evaluated based on the responses of the samples to a water bath shaker at 80 °C. For one hour, dried CS-ZL/ZrO/Fe<sub>3</sub>O<sub>4</sub> was soaked in HCl and  $\text{H}_2\text{SO}_4$  concentrations ranging from 0.01 to 0.1 M. Following that, the sample was dried in an oven at 60 °C for twenty-four hours. The calculation of the dry weight retention (WR) was performed using Equation (19).

$$\text{WR} (\%) = \frac{w_i}{w_a} \times 100 \quad (19)$$

where  $w_i$  and  $w_a$  are the dry weights of CS-ZL/ZrO/Fe<sub>3</sub>O<sub>4</sub> before and after treatment, respectively.

### 3.11. Characterization of CS-ZL/ZrO/Fe<sub>3</sub>O<sub>4</sub>

The crystalline structure of CS-ZL/ZrO/Fe<sub>3</sub>O<sub>4</sub> was analyzed using a powder X-ray diffractometer (XRD) equipped with Cu/K $\alpha$  radiation (Hypix-3000). Fourier transform

infrared spectra (FTIR) of CS-ZL/ZrO/Fe<sub>3</sub>O<sub>4</sub> were measured before and after PO<sub>4</sub><sup>3-</sup> adsorption using a Thermo Scientific Nicolet iS10 instrument (Thermo Fisher Scientific Inc., Waltham, MA, USA). The ATR-FTIR approach was used to analyze samples with a resolution of 4 cm<sup>-1</sup> throughout the wavenumber spectrum spanning 400–4000 cm<sup>-1</sup>. To determine the specific surface area (SSA), the BET approach was combined with a surface area analyzer (MicroActive AutoPore V 9600 2.03.00, Micromeritics, Norcross, GA, USA). SEM-EDS (JIED-2300, Shimadzu, Kyoto, Japan) was used to examine the SEM images and the elemental distributions of CS-ZL/ZrO/Fe<sub>3</sub>O<sub>4</sub>. The initial (pHi) and final (pHf) pH values of the solutions were measured to determine the surface charge over a range of pH values (pH<sub>ZPC</sub>). The pHi was adjusted from 2.0 to 10.0 in 0.01 M NaCl solution. Following that, 0.1 g of CS-ZL/ZrO/Fe<sub>3</sub>O<sub>4</sub> was added and stirred for 24 h at 30 °C, and pHf was measured. A plot of ΔpH = pHf – pHi vs. pHi was used to determine pH<sub>ZPC</sub>, which corresponds to the neutral surface charge.

### 3.12. Data Analysis

All results were noted and edited using Microsoft Excel. The effects of coexisting ions on PO<sub>4</sub><sup>3-</sup> removal were examined using a completely randomized design (CRD). Data were analyzed using ANOVA with Tukey's test ( $p \leq 0.05$ ) using Minitab 21.3.1.

## 4. Conclusions

In this study, a novel adsorbent, CS-ZL/ZrO/Fe<sub>3</sub>O<sub>4</sub>, was prepared from chitosan (CS), zeolite (ZL), ZrO, and magnetite (Fe<sub>3</sub>O<sub>4</sub>) via a crosslinking approach. The Box–Behnken design (BBD) and the response surface methodology (RSM), with their corresponding four separate factors (pH, dosage, temperature, and time), were used to develop the best experimental conditions for PO<sub>4</sub><sup>3-</sup> removal. Weight retention (WR) was measured in a batch reactor under acidic conditions (HCl and H<sub>2</sub>SO<sub>4</sub>) at 80 °C for 1 h to determine the mechanical stability. The results indicate that CS-ZL/ZrO/Fe<sub>3</sub>O<sub>4</sub> was stable and did not change in the functional group peak area after treatment. The best conditions were at a pH of 2.0, with an adsorption capacity and percentage removal of 732.56 mg/g and 87.91%, respectively. The Freundlich isotherm and pseudo-second-order (PSO) kinetic models were fitted to PO<sub>4</sub><sup>3-</sup> removal, indicating heterogeneous and chemical sorption. In addition, the results suggest that PO<sub>4</sub><sup>3-</sup> adsorption occurred via the electrostatic interactions between the positive charge of CS-ZL/ZrO/Fe<sub>3</sub>O<sub>4</sub> and the negative charge of H<sub>2</sub>PO<sub>4</sub><sup>4-</sup> as well as ion exchange and hydrogen bonding. The presence of coexisting ions (Mg<sup>2+</sup>, Ca<sup>2+</sup>, CO<sub>3</sub><sup>2-</sup>, SO<sub>4</sub><sup>2-</sup>, and Na<sup>+</sup>) had no effect on the removal of PO<sub>4</sub><sup>3-</sup> ( $p \leq 0.05$ ). The desorption studies revealed that 1 M NaOH was better at releasing PO<sub>4</sub><sup>3-</sup>, reaching 95.77% after 30 min of treatment at 30 °C. The reusability of CS-ZL/ZrO/Fe<sub>3</sub>O<sub>4</sub> showed good performance over three cycles. These findings imply that CS-ZL/ZrO/Fe<sub>3</sub>O<sub>4</sub> is the best way to improve the stability of chitosan under acidic conditions, and it is a good adsorbent for removing PO<sub>4</sub><sup>3-</sup> and other potential water pollutants from water.

**Author Contributions:** Conceptualization, E.H.; Methodology, E.H.; Validation, Y.M.; Formal analysis, E.H.; Investigation, E.H. and Y.M.; Data curation, S.Y.; Writing—original draft, E.H.; Writing—review & editing, E.H. and N.M.B.M.S.; Visualization, H.H.; Supervision, S.Y., Y.M. and H.H.; Project administration, H.H. All authors have read and agreed to the published version of the manuscript.

**Funding:** This research received no external funding.

**Data Availability Statement:** Not applicable.

**Acknowledgments:** The author (E.H.) would like to express gratitude to the MEXT Scholarship for the funding received while studying at the Prefectural University of Hiroshima in Japan.

**Conflicts of Interest:** The authors declare no conflict of interest.

## References

1. Yoon, S.-Y.; Lee, C.-G.; Park, J.-A.; Kim, J.-H.; Kim, S.-B.; Lee, S.-H.; Choi, J.-W. Kinetic, equilibrium and thermodynamic studies for phosphate adsorption to magnetic iron oxide nanoparticles. *Chem. Eng. J.* **2014**, *236*, 341–347. [[CrossRef](#)]
2. Chen, M.; Ding, S.; Chen, X.; Sun, Q.; Fan, X.; Lin, J.; Ren, M.; Yang, L.; Zhang, C. Mechanisms driving phosphorus release during algal blooms based on hourly changes in iron and phosphorus concentrations in sediments. *Water Res.* **2018**, *133*, 153–164. [[CrossRef](#)] [[PubMed](#)]
3. Schindler, D.W.; Carpenter, S.R.; Chapra, S.C.; Hecky, R.E.; Orihel, D.M. Reducing phosphorus to curb lake eutrophication is a success. *Environ. Sci. Technol.* **2016**, *50*, 8923–8929. [[CrossRef](#)]
4. Pawar, R.R.; Gupta, P.; Lalmunsiam; Bajaj, H.C.; Lee, S.-M. Al-intercalated acid activated bentonite beads for the removal of aqueous phosphate. *Sci. Total Environ.* **2016**, *572*, 1222–1230. [[CrossRef](#)]
5. Xie, Q.; Li, Y.; Lv, Z.; Zhou, H.; Yang, X.; Chen, J.; Guo, H. Effective Adsorption and Removal of Phosphate from Aqueous Solutions and Eutrophic Water by Fe-based MOFs of MIL-101. *Sci. Rep.* **2017**, *7*, 3316. [[CrossRef](#)] [[PubMed](#)]
6. Wei, W.; Du, J.; Li, J.; Yan, M.; Zhu, Q.; Jin, X.; Zhu, X.; Hu, Z.; Tang, Y.; Lu, Y. Construction of Robust Enzyme Nanocapsules for Effective Organophosphate Decontamination, Detoxification, and Protection. *Adv. Mater.* **2013**, *25*, 2212–2218. [[CrossRef](#)]
7. Wang, F.; Wei, J.; Zou, X.; Fu, R.; Li, J.; Wu, D.; Lv, H.; Zhu, G.; Wu, X.; Chen, H. Enhanced electrochemical phosphate recovery from livestock wastewater by adjusting pH with plant ash. *J. Environ. Manag.* **2019**, *250*, 109473. [[CrossRef](#)]
8. Ren, Y.; Zheng, W.; Duan, X.; Goswami, N.; Liu, Y. Recent advances in electrochemical removal and recovery of phosphorus from water: A review. *Environ. Funct. Mater.* **2022**, *1*, 10–20. [[CrossRef](#)]
9. Hidayat, E.; Harada, H. Simultaneously Recovery of Phosphorus and Potassium Using Bubble Column Reactor as Struvite-K and Implementation on Crop Growth. In *Crystallization and Applications*; IntechOpen: London, UK, 2022. [[CrossRef](#)]
10. Guida, S.; Rubertelli, G.; Jefferson, B.; Soares, A. Demonstration of ion exchange technology for phosphorus removal and recovery from municipal wastewater. *Chem. Eng. J.* **2021**, *420*, 129913. [[CrossRef](#)]
11. Hidayat, E.; Yoshino, T.; Yonemura, S.; Mitoma, Y.; Harada, H. A Carbonized Zeolite/Chitosan Composite as an Adsorbent for Copper (II) and Chromium (VI) Removal from Water. *Materials* **2023**, *16*, 2532. [[CrossRef](#)]
12. Zahari, K.F.A.; Sahu, U.K.; Khadiran, T.; Surip, S.N.; Allothman, Z.A.; Jawad, A.H. Mesoporous Activated Carbon from Bamboo Waste via Microwave-Assisted K<sub>2</sub>CO<sub>3</sub> Activation: Adsorption Optimization and Mechanism for Methylene Blue Dye. *Separations* **2022**, *9*, 390. [[CrossRef](#)]
13. Matei, A.; Racoviteanu, G. Review of the technologies for nitrates removal from water intended for human consumption. In *IOP Conference Series: Earth and Environmental Science*; IOP Publishing Ltd.: Bristol, UK, 2021. [[CrossRef](#)]
14. Rodrigues, L.A.; da Silva, M.L.C.P. An investigation of phosphate adsorption from aqueous solution onto hydrous niobium oxide prepared by co-precipitation method. *Colloids Surf. A Physicochem. Eng. Asp.* **2009**, *334*, 191–196. [[CrossRef](#)]
15. Huang, W.; Zhang, Y.; Li, D. Adsorptive removal of phosphate from water using mesoporous materials: A review. In *Journal of Environmental Management*; Academic Press: Cambridge, MA, USA, 2017; Volume 193, pp. 470–482.
16. Blaney, L.; Cinar, S.; Sengupta, A.K. Hybrid anion exchanger for trace phosphate removal from water and wastewater. *Water Res.* **2007**, *41*, 1603–1613. [[CrossRef](#)] [[PubMed](#)]
17. Hidayat, E.; Yoshino, T.; Yonemura, S.; Mitoma, Y.; Harada, H. Synthesis, Adsorption Isotherm and Kinetic Study of Alkaline-Treated Zeolite/Chitosan/Fe<sup>3+</sup> Composites for Nitrate Removal from Aqueous Solution—Anion and Dye Effects. *Gels* **2022**, *8*, 782. [[CrossRef](#)] [[PubMed](#)]
18. Almasri, D.A.; Saleh, N.B.; Atieh, M.A.; McKay, G.; Ahzi, S. Adsorption of phosphate on iron oxide doped halloysite nanotubes. *Sci. Rep.* **2019**, *9*, 3232. [[CrossRef](#)] [[PubMed](#)]
19. Ladeira, N.M.B.; Donnici, C.L.; de Mesquita, J.P.; Pereira, F.V. Preparation and characterization of hydrogels obtained from chitosan and carboxymethyl chitosan. *J. Polym. Res.* **2021**, *28*, 335. [[CrossRef](#)]
20. Mohammed, I.A.; Malek, N.N.A.; Jawad, A.H.; Mastuli, M.S.; Allothman, Z.A. Box–Behnken Design for Optimizing Synthesis and Adsorption Conditions of Covalently Crosslinked Chitosan/Coal Fly Ash Composite for Reactive Red 120 Dye Removal. *J. Polym. Environ.* **2022**, *30*, 3447–3462. [[CrossRef](#)]
21. Jawad, A.H.; Hameed, B.H.; Abdulhameed, A.S. Synthesis of biohybrid magnetic chitosan-polyvinyl alcohol/MgO nanocomposite blend for remazol brilliant blue R dye adsorption: Solo and collective parametric optimization. *Polym. Bull.* **2022**, *80*, 4927–4947. [[CrossRef](#)]
22. Aramesh, N.; Bagheri, A.R.; Bilal, M. Chitosan-based hybrid materials for adsorptive removal of dyes and underlying interaction mechanisms. In *International Journal of Biological Macromolecules*; Elsevier B.V.: Amsterdam, The Netherlands, 2021; Volume 183, pp. 399–422. [[CrossRef](#)]
23. Salehi, S.; Anbia, M. Adsorption Selectivity of CO<sub>2</sub> and CH<sub>4</sub> on Novel PANI/Alkali-Exchanged FAU Zeolite Nanocomposites. *J. Inorg. Organomet. Polym. Mater.* **2017**, *27*, 1281–1291. [[CrossRef](#)]
24. Hidayat, E.; Yonemura, S.; Mitoma, Y.; Harada, H. Methylene Blue Removal by Chitosan Cross-Linked Zeolite from Aqueous Solution and Other Ion Effects: Isotherm, Kinetic, and Desorption Studies. *Adsorpt. Sci. Technol.* **2022**, *2022*, 1853758. [[CrossRef](#)]
25. Hidayat, E.; Harada, H.; Mitoma, Y.; Yonemura, S.; A Halem, H.I. Rapid Removal of Acid Red 88 by Zeolite/Chitosan Hydrogel in Aqueous Solution. *Polymers* **2022**, *14*, 893. [[CrossRef](#)]
26. Vakili, M.; Qiu, W.; Cagnetta, G.; Huang, J.; Yu, G. Mechanochemically oxidized chitosan-based adsorbents with outstanding Penicillin G adsorption capacity. *J. Environ. Chem. Eng.* **2021**, *9*, 105454. [[CrossRef](#)]

27. Gao, Y.; Bao, S.; Zhang, L.; Zhang, L. Nitrate removal by using chitosan/zeolite molecular sieves composite at low temperature: Characterization, mechanism, and regeneration studies. *Desalination Water Treat* **2020**, *203*, 160–171. [[CrossRef](#)]
28. Lin, J.; Zhan, Y. Adsorption of humic acid from aqueous solution onto unmodified and surfactant-modified chitosan/zeolite composites. *Chem. Eng. J.* **2012**, *200–202*, 202–213. [[CrossRef](#)]
29. Mohammad, A.K.T.; Abdulhameed, A.S.; Jawad, A.H. Box-Behnken design to optimize the synthesis of new crosslinked chitosan-glyoxal/TiO<sub>2</sub> nanocomposite: Methyl orange adsorption and mechanism studies. *Int. J. Biol. Macromol.* **2019**, *129*, 98–109. [[CrossRef](#)] [[PubMed](#)]
30. Nga, N.K.; Chau, N.T.T.; Viet, P.H. Preparation and characterization of a chitosan/MgO composite for the effective removal of reactive blue 19 dye from aqueous solution. *J. Sci. Adv. Mater. Devices* **2020**, *5*, 65–72. [[CrossRef](#)]
31. Spoială, A.; Ilie, C.-I.; Dolete, G.; Croitoru, A.-M.; Surdu, V.-A.; Truşcă, R.-D.; Motelica, L.; Oprea, O.-C.; Ficaï, D.; Ficaï, A.; et al. Preparation and Characterization of Chitosan/TiO<sub>2</sub> Composite Membranes as Adsorbent Materials for Water Purification. *Membranes* **2022**, *12*, 804. [[CrossRef](#)]
32. Reghioua, A.; Barkat, D.; Jawad, A.H.; Abdulhameed, A.S.; Rangabhashiyam, S.; Khan, M.R.; Alothman, Z.A. Magnetic Chitosan-Glutaraldehyde/Zinc Oxide/Fe<sub>3</sub>O<sub>4</sub> Nanocomposite: Optimization and Adsorptive Mechanism of Remazol Brilliant Blue R Dye Removal. *J. Polym. Environ.* **2021**, *29*, 3932–3947. [[CrossRef](#)]
33. Reghioua, A.; Barkat, D.; Jawad, A.H.; Abdulhameed, A.S.; Khan, M.R. Synthesis of Schiff's base magnetic crosslinked chitosan-glyoxal/ZnO/Fe<sub>3</sub>O<sub>4</sub> nanoparticles for enhanced adsorption of organic dye: Modeling and mechanism study. *Sustain. Chem. Pharm.* **2021**, *20*, 100379. [[CrossRef](#)]
34. Cho, D.-W.; Jeon, B.-H.; Jeong, Y.; Nam, I.-H.; Choi, U.-K.; Kumar, R.; Song, H. Synthesis of hydrous zirconium oxide-impregnated chitosan beads and their application for removal of fluoride and lead. *Appl. Surf. Sci.* **2016**, *372*, 13–19. [[CrossRef](#)]
35. Sathiyavimal, S.; Vasantharaj, S.; Kaliannan, T.; Pugazhendhi, A. Eco-biocompatibility of chitosan coated biosynthesized copper oxide nanocomposite for enhanced industrial (Azo) dye removal from aqueous solution and antibacterial properties. *Carbohydr. Polym.* **2020**, *241*, 116243. [[CrossRef](#)]
36. Salehi, S.; Alijani, S.; Anbia, M. Enhanced adsorption properties of zirconium modified chitosan-zeolite nanocomposites for vanadium ion removal. *Int. J. Biol. Macromol.* **2020**, *164*, 105–120. [[CrossRef](#)] [[PubMed](#)]
37. Rosales, E.; Anasie, D.; Pazos, M.; Lazar, I.; Sanromán, M.A. Kaolinite adsorption-regeneration system for dyestuff treatment by Fenton based processes. *Sci. Total Environ.* **2018**, *622–623*, 556–562. [[CrossRef](#)] [[PubMed](#)]
38. Ghobadi, M.; Gharabaghi, M.; Abdollahi, H.; Boroumand, Z.; Moradian, M. MnFe<sub>2</sub>O<sub>4</sub>-graphene oxide magnetic nanoparticles as a high-performance adsorbent for rare earth elements: Synthesis, isotherms, kinetics, thermodynamics and desorption. *J. Hazard. Mater.* **2018**, *351*, 308–316. [[CrossRef](#)]
39. Maksud, M.I.A.A.; Elgarahy, A.M.; Farrell, C.; Al-Muhtaseb, A.H.; Rooney, D.W.; Osman, A.I. Insight on water remediation application using magnetic nanomaterials and biosorbents. In *Coordination Chemistry Reviews*; Elsevier B.V.: Amsterdam, The Netherlands, 2020; Volume 403.
40. Fu, Z.; Li, H.; Yang, L.; Yuan, H.; Jiao, Z.; Chen, L.; Huang, J.; Liu, Y.-N. Magnetic polar post-cross-linked resin and its adsorption towards salicylic acid from aqueous solution. *Chem. Eng. J.* **2015**, *273*, 240–246. [[CrossRef](#)]
41. Al-Harahsheh, M.; AlJarrah, M.; Mayyas, M.; Alrebaki, M. High-stability polyamine/amide-functionalized magnetic nanoparticles for enhanced extraction of uranium from aqueous solutions. *J. Taiwan Inst. Chem. Eng.* **2018**, *86*, 148–157. [[CrossRef](#)]
42. Zong, E.; Shen, Y.; Yang, J.; Liu, X.; Song, P. Preparation and Characterization of an Invasive Plant-Derived Biochar-Supported Nano-Sized Lanthanum Composite and Its Application in Phosphate Capture from Aqueous Media. *ACS Omega* **2023**, *8*, 14177–14189. [[CrossRef](#)]
43. Mekonnen, D.T.; Alemayehu, E.; Lennartz, B. Removal of Phosphate Ions from Aqueous Solutions by Adsorption onto Leftover Coal. *Water* **2020**, *12*, 1381. [[CrossRef](#)]
44. Zhang, M.; Zhang, Z.; Peng, Y.; Feng, L.; Li, X.; Zhao, C.; Sarfaraz, K. Novel cationic polymer modified magnetic chitosan beads for efficient adsorption of heavy metals and dyes over a wide pH range. *Int. J. Biol. Macromol.* **2020**, *156*, 289–301. [[CrossRef](#)]
45. Safaei-Ghomi, J.; Tavazo, M.; Shahbazi-Alavi, H. Chitosan-attached nano-Fe<sub>3</sub>O<sub>4</sub> as a superior and retrievable heterogeneous catalyst for the synthesis of benzopyranophenazines using chitosan-attached nano-Fe<sub>3</sub>O<sub>4</sub>. *Z. Fur Nat.—Sect. B J. Chem. Sci.* **2019**, *74*, 733–738. [[CrossRef](#)]
46. Annaduzzaman, M.; Bhattacharya, P.; Ersoz, M.; Lazarova, Z. Characterization of a chitosan biopolymer and arsenate removal for drinking water treatment. In *One Century of the Discovery of Arsenicosis in Latin America (1914–2014): As 2014—Proceedings of the 5th International Congress on Arsenic in the Environment*; CRC Press/Balkema: Boca Raton, FL, USA, 2014; pp. 745–747.
47. Yang, T.; Zhang, W.; Liu, H.; Guo, Y. Enhanced removal of U(VI) from aqueous solution by chitosan-modified zeolite. *J. Radioanal. Nucl. Chem.* **2020**, *323*, 1003–1012. [[CrossRef](#)]
48. Fajardo, A.R.; Lopes, L.C.; Pereira, A.G.; Rubira, A.F.; Muniz, E.C. Polyelectrolyte complexes based on pectin-NH<sub>2</sub> and chondroitin sulfate. *Carbohydr. Polym.* **2012**, *87*, 1950–1955. [[CrossRef](#)]
49. Zhang, S.; Zhang, Y.; Fu, L.; Jing, M. A chitosan fiber as green material for removing Cr(VI) ions and Cu(II) ions pollutants. *Sci. Rep.* **2021**, *11*, 22942. [[CrossRef](#)] [[PubMed](#)]
50. Cui, Z.; Xiang, Y.; Si, J.; Yang, M.; Zhang, Q.; Zhang, T. Ionic interactions between sulfuric acid and chitosan membranes. *Carbohydr. Polym.* **2008**, *73*, 111–116. [[CrossRef](#)]
51. Bouchet, R.; Siebert, E. Proton conduction in acid doped polybenzimidazole. *Solid State Ion.* **1999**, *118*, 287–299. [[CrossRef](#)]

52. Miraboutalebi, S.M.; Nikouzad, S.K.; Peydayesh, M.; Allahgholi, N.; Vafajoo, L.; McKay, G. Methylene blue adsorption via maize silk powder: Kinetic, equilibrium, thermodynamic studies and residual error analysis. *Process. Saf. Environ. Prot.* **2017**, *106*, 191–202. [[CrossRef](#)]
53. Jembere, A.L.; Genet, M.B. Comparative adsorptive performance of adsorbents developed from sugar industrial wastes for the removal of melanoidin pigment from molasses distillery spent wash. *Water Resour. Ind.* **2021**, *26*, 100165. [[CrossRef](#)]
54. Lin, B.; Hua, M.; Zhang, Y.; Zhang, W.; Lv, L.; Pan, B. Effects of organic acids of different molecular size on phosphate removal by HZO-201 nanocomposite. *Chemosphere* **2017**, *166*, 422–430. [[CrossRef](#)]
55. Li, R.; Wang, J.J.; Zhou, B.; Awasthi, M.K.; Ali, A.; Zhang, Z.; Lahori, A.H.; Mahar, A. Recovery of phosphate from aqueous solution by magnesium oxide decorated magnetic biochar and its potential as phosphate-based fertilizer substitute. *Bioresour. Technol.* **2016**, *215*, 209–214. [[CrossRef](#)]
56. Shen, H.; Wang, Z.; Zhou, A.; Chen, J.; Hu, M.; Dong, X.; Xia, Q. Adsorption of phosphate onto amine functionalized nano-sized magnetic polymer adsorbents: Mechanism and magnetic effects. *RSC Adv.* **2015**, *5*, 22080–22090. [[CrossRef](#)]
57. Jung, K.W.; Lee, S.; Lee, Y.J. Synthesis of novel magnesium ferrite (MgFe<sub>2</sub>O<sub>4</sub>)/biochar magnetic composites and its adsorption behavior for phosphate in aqueous solutions. *Bioresour. Technol.* **2017**, *245*, 751–759. [[CrossRef](#)] [[PubMed](#)]
58. Lai, L.; Xie, Q.; Chi, L.; Gu, W.; Wu, D. Adsorption of phosphate from water by easily separable Fe<sub>3</sub>O<sub>4</sub>@SiO<sub>2</sub> core/shell magnetic nanoparticles functionalized with hydrous lanthanum oxide. *J. Colloid Interface Sci.* **2016**, *465*, 76–82. [[CrossRef](#)] [[PubMed](#)]
59. Trinh, V.T.; Nguyen, T.M.P.; Van, H.T.; Hoang, L.P.; Nguyen, T.V.; Ha, L.T.; Vu, X.H.; Pham, T.T.; Quang, N.V.; Nguyen, X.C. Phosphate Adsorption by Silver Nanoparticles-Loaded Activated Carbon derived from Tea Residue. *Sci. Rep.* **2020**, *10*, 3634. [[CrossRef](#)]
60. Su, Y.; Yang, W.; Sun, W.; Li, Q.; Shang, J.K. Synthesis of mesoporous cerium–zirconium binary oxide nanoadsorbents by a solvothermal process and their effective adsorption of phosphate from water. *Chem. Eng. J.* **2015**, *268*, 270–279. [[CrossRef](#)]
61. Huang, W.; Chen, J.; He, F.; Tang, J.; Li, D.; Zhu, Y.; Zhang, Y. Effective phosphate adsorption by Zr/Al-pillared montmorillonite: Insight into equilibrium, kinetics and thermodynamics. *Appl. Clay Sci.* **2014**, *104*, 252–260. [[CrossRef](#)]
62. Deng, Z.; Gu, S.; Cheng, H.; Xing, D.; Twagirayezu, G.; Wang, X.; Ning, W.; Mao, M. Removal of Phosphate from Aqueous Solution by Zeolite-Biochar Composite: Adsorption Performance and Regulation Mechanism. *Appl. Sci.* **2022**, *12*, 5334. [[CrossRef](#)]
63. Shukla, S.K.; Pandey, S.; Saha, S.; Singh, H.R.; Mishra, P.K.; Kumar, S.; Jha, S.K. Removal of crystal violet by Cu-chitosan nano-biocomposite particles using Box–Behnken design. *J. Environ. Chem. Eng.* **2021**, *9*, 105847. [[CrossRef](#)]
64. Hidayat, E.; Khaekhum, S.; Yonemura, S.; Mitoma, Y.; Harada, H. Biosorption of Eriochrome Black T Using *Exserohilum rostratum* NMS1.5 Mycelia Biomass. *J* **2022**, *5*, 427–434. [[CrossRef](#)]

**Disclaimer/Publisher’s Note:** The statements, opinions and data contained in all publications are solely those of the individual author(s) and contributor(s) and not of MDPI and/or the editor(s). MDPI and/or the editor(s) disclaim responsibility for any injury to people or property resulting from any ideas, methods, instructions or products referred to in the content.